Fundamental Research xxx (xxxx) xxx

Contents lists available at ScienceDirect

Fundamental Research

journal homepage: http://www.keaipublishing.com/en/journals/fundamental-research/

Article

Ternary NiCoTi-layered double hydroxide nanosheets as a pH-responsive nanoagent for photodynamic/chemodynamic synergistic therapy

Tingting Hu[a,1], Zhan Zhou[b,1], Jiajia Zha[c], Gareth R. Williams[d], Zhikang Wu[e], Wei Zhao[a], Weicheng Shen[a], Hai Li[e], Xisheng Weng[f,*], Ruizheng Liang[a,*], Chaoliang Tan[c,g,h,*]

[a] State Key Laboratory of Chemical Resource Engineering, Beijing Advanced Innovation Center for Soft Matter Science and Engineering, Beijing University of Chemical Technology, Beijing 100029, China
[b] College of Chemistry and Chemical Engineering, Henan Key Laboratory of Function-Oriented Porous Materials, Luoyang Normal University, Luoyang 471934, China
[c] Department of Electrical Engineering, City University of Hong Kong, 83 Tat Chee Avenue, Kowloon, Hong Kong SAR, China
[d] UCL School of Pharmacy, University College London, 29-39 Brunswick Square, London, WC1N 1AX, United Kingdom
[e] Institute of Advanced Materials (IAM) and Key Laboratory of Flexible Electronics (KLoFE), Nanjing Tech University (NanjingTech), 30 South Puzhu Road, Nanjing 211816, China
[f] Department of Orthopedic Surgery, State Key Laboratory of Complex Severe and Rare Diseases, Peking Union Medical College Hospital, Chinese Academy of Medical Science and Peking Union Medical College, Beijing 100730, China
[g] Center of Super-Diamond and Advanced Films (COSDAF), City University of Hong Kong, Kowloon, Hong Kong SAR, China
[h] Shenzhen Research Institute, City University of Hong Kong, Shenzhen 518057, China

ARTICLE INFO

Article history:
Received 16 April 2022
Received in revised form 18 May 2022
Accepted 5 June 2022
Available online xxx

Keywords:
Layered double hydroxides
Photodynamic therapy
pH-responsive
Chemodynamic therapy
Oxygen vacancy

ABSTRACT

Combining photodynamic therapy (PDT) with chemodynamic therapy (CDT) has been proven to be a promising strategy to improve the treatment efficiency of cancer, because of the synergistic therapeutic effect arising between the two modalities. Herein, we report an inorganic nanoagent based on ternary NiCoTi-layered double hydroxide (NiCoTi-LDH) nanosheets to realize highly efficient photodynamic/chemodynamic synergistic therapy. The NiCoTi-LDH nanosheets exhibit oxygen vacancy-promoted electron-hole separation and photogenerated hole-induced O_2-independent reactive oxygen species (ROS) generation under acidic circumstances, realizing *in situ* pH-responsive PDT. Moreover, due to the effective conversion between Co^{3+} and Co^{2+} caused by photogenerated electrons, the NiCoTi-LDH nanosheets catalyze the release of hydroxyl radicals (•OH) from H_2O_2 through Fenton reactions, resulting in CDT. Laser irradiation enhances the catalyzed ability of the NiCoTi-LDH nanosheets to promote the ROS generation, resulting in a better performance than TiO_2 nanoparticles at pH 6.5. *In vitro* and *in vivo* experimental results show conclusively that NiCoTi-LDH nanosheets plus irradiation lead to efficient cell apoptosis and significant inhibition of tumor growth. This study reports a new pH-responsive inorganic nanoagent with oxygen vacancy-promoted photodynamic/chemodynamic synergistic performance, offering a potentially appealing clinical strategy for selective tumor elimination.

1. Introduction

Chemodynamic therapy (CDT) is an emerging therapeutic modality for the treatment of cancer. Interest in CDT has bloomed in recent years owning to its minimal invasiveness, tumor-specificity and minimal side effects [1–3]. CDT uses Fenton or Fenton-like reactions to generate highly oxidative hydroxyl radicals (•OH) from endogenous hydrogen peroxide (H_2O_2), thereby inducing cancer cell apoptosis or necrosis [4–6]. Regrettably, the curative effect of CDT is hampered by the low efficiency of the Fenton reaction [7,8]. To realize the desired antitumor effect, CDT usually needs to be combined with other therapeutic methods. Photodynamic therapy (PDT) is another kind of reactive oxygen species (ROS)-based therapeutic modality with high selectivity and spatiotemporal accuracy, and which is not susceptible to the emergence of drug resistance [9,10]. PDT adopts light-excited photosensitizers (PSs) to generate ROS including ·OH, superoxide radicals ($\cdot O_2^-$) and singlet oxygen ($^1O_2$) [11,12]. It has been reported that ultraviolet (UV)/visible laser irradiation can improve •OH generation efficiency in Fenton reactions to enhance the antitumor effect of CDT [13–15]. For example, the Fenton reaction catalyzed by biotite nanosheets could be significantly enhanced under 650 nm light irradiation [16]. Therefore, the combination of CDT and PDT has proven to be a promising

* Corresponding author.
E-mail addresses: drwengxsh@163.com (X. Weng), liangruizheng2000@163.com (R. Liang), chaoltan@cityu.edu.hk (C. Tan).
[1] These authors contributed equally to this work.

https://doi.org/10.1016/j.fmre.2022.06.001

Please cite this article as: T. Hu, Z. Zhou, J. Zha et al., Ternary NiCoTi-layered double hydroxide nanosheets as a pH-responsive nanoagent for photodynamic/chemodynamic synergistic therapy, Fundamental Research, https://doi.org/10.1016/j.fmre.2022.06.001

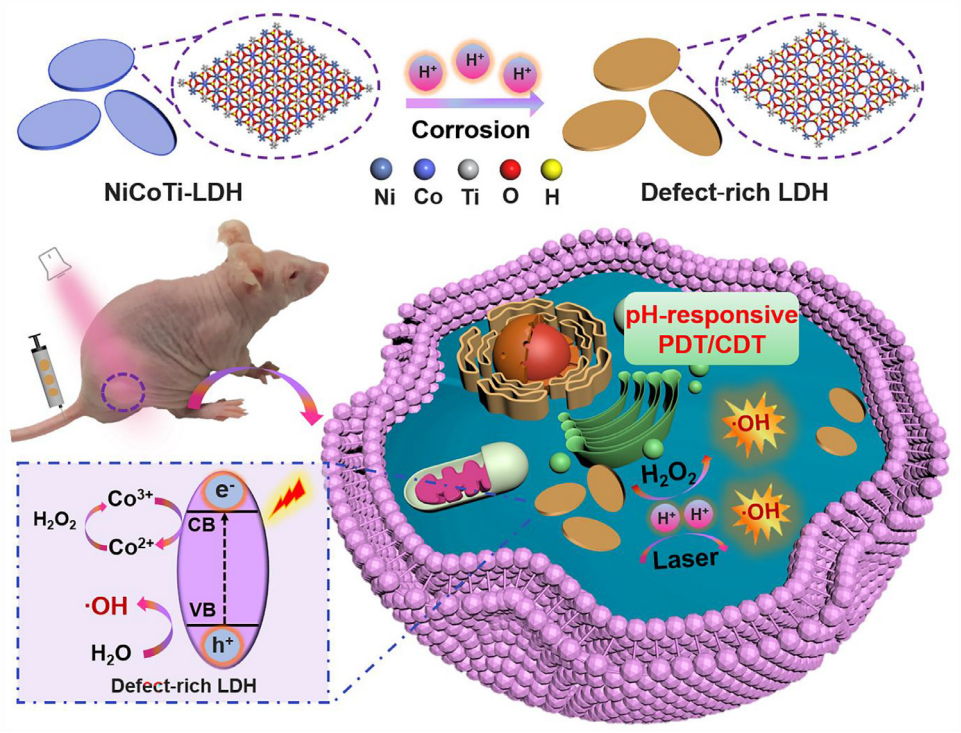

Scheme 1. Schematic illustration of pH-responsive PDT/CDT synergistic treatment in the presence of NiCoTi-LDH.

strategy to realize enhanced anticancer performance. However, most of the reported nanoagents for CDT/PDT synergistic therapy involve complex designs or incorporation of PSs and Fenton agents, such as manganese ferrite nanoparticle-anchored mesoporous silica nanoparticles loaded with chlorin e6 [17], Cu^{2+}-graphitic carbon nitride ($g\text{-}C_3N_4$) nanosheets [18], and $NaYF_4$:Yb^{3+},Tm^{3+}@$mSiO_2$-Ru^{2+}/Fe^{2+} nanoplatform [19]. Therefore, achieving synergistic CDT/PDT in a single smart nanoagent remains a formidable challenge.

Because of their diverse chemical composition, easy preparation, excellent stability and biocompatibility, two-dimensional (2D) layered double hydroxides (LDHs) have been demonstrated to be promising nanoagents in biomedical fields including drug delivery, bioimaging and cancer therapy [20–23]. For example, ultrathin Gd-doped MgAl-LDH nanosheets can be used as a carrier to co-load with doxorubicin and indocyanine green for fluorescence/magnetic resonance imaging guided cancer therapy [24]. CoFe-LDH and CuFe-LDH nanosheets can trigger the Fenton reaction to realize CDT by exploiting the abundant H_2O_2 in cancer cells and converting this into ·OH within the tumor microenvironment [25,26]. Moreover, isophthalic acid-intercalated ZnAl-LDHs with a high $^1O_2$ quantum yield can be adopted as a composite PS for PDT [27]. Despite the fact that 2D LDHs have been used as the Fenton agents for high-efficiency CDT, or as the host to load with organic PSs for enhanced PDT, no one has reported the direct utilization of 2D LDH nanosheets themselves for CDT/PDT synergistic therapy.

Herein, we report a new nanoagent based on ternary NiCoTi-LDH which can provide pH-responsive and high-efficient CDT/PDT synergistic therapy (Scheme 1). Specifically, a large number of oxygen vacancies (OVs) on NiCoTi-LDH nanosheets could be produced in acidic circumstances. The OVs on NiCoTi-LDH nanosheets caused by corrosion can facilitate the effective separation of electron-hole pairs. To this end, the NiCoTi-LDH nanosheets can be used as a PS for *in situ* pH-responsive PDT since they exhibit OV-promoted electron-hole separation and photogenerated hole-induced O_2-independent ROS generation under acidic circumstances. Importantly, because of the photogenerated electron-induced effective conversion between Co^{3+} and Co^{2+}, the NiCoTi-LDH nanosheets can also catalyze the H_2O_2 to generate highly toxic •OH through the Fenton reaction. Note that laser irradiation increases the ability of the NiCoTi-LDH nanosheets to catalyze ROS generation under acidic conditions and the performance is better than that of TiO_2 nanoparticles at pH 6.5. *In vitro* and *in vivo* tests proved conclusively that the NiCoTi-LDH nanosheets plus irradiation lead to efficient cell apoptosis and significant inhibition of tumor growth through the CDT/PDT synergistic therapy. This study reports a new pH-responsive inorganic nanoagent with OV-promoted synergistic CDT/PDT performance, offering a potentially appealing strategy for design of highly efficient multifunctional biomedical nanoagents.

2. Results and discussion

Ternary NiCoTi-LDH nanosheets were synthesized by a low-temperature wet-chemical synthesis method on the basis of a previously reported approach with slight modifications (see Experimental Section in the Supporting Information) [24]. As shown in Fig. 1a, the transmission electron microscope (TEM) image reveals discrete NiCoTi-LDH nanosheets with a size of 50–80 nm. High-resolution TEM (HRTEM) image of a typical NiCoTi-LDH nanosheet shows a continuous lattice fringe and measured lattice distance of ~ 0.151 nm (inset of Fig. 1a), corresponding to the (110) plane of NiCoTi-LDH. The elemental composition of the nanosheets was characterized by energy dispersive spectroscopic (EDS) element mapping (Fig. 1b). This confirms the presence of Ni, Co, Ti and O and their homogenous distribution through the entire nanosheet. The thickness of the nanosheets was characterized by atomic force microscopy (AFM) and found to be 2.5–4.5 nm (Fig. 1c). According to the X-ray powder diffraction (XRD) pattern in Fig. 1d, all the characteristic diffraction peaks are well matched with the reference [28], confirming its crystal structure. Dynamic light scattering (DLS) shows that the hydrodynamic diameters of NiCoTi-LDH nanosheets are 83.4 ± 3.8 nm, 85.5 ± 4.3 nm, and 94.2 ± 5.0 nm in water, culture medium and phosphate buffer saline (PBS), respectively (Fig. 1e). There is no significant change in hydrodynamic dimension over one week, demonstrating that the colloid has a good stability (Fig. 1f). Digital

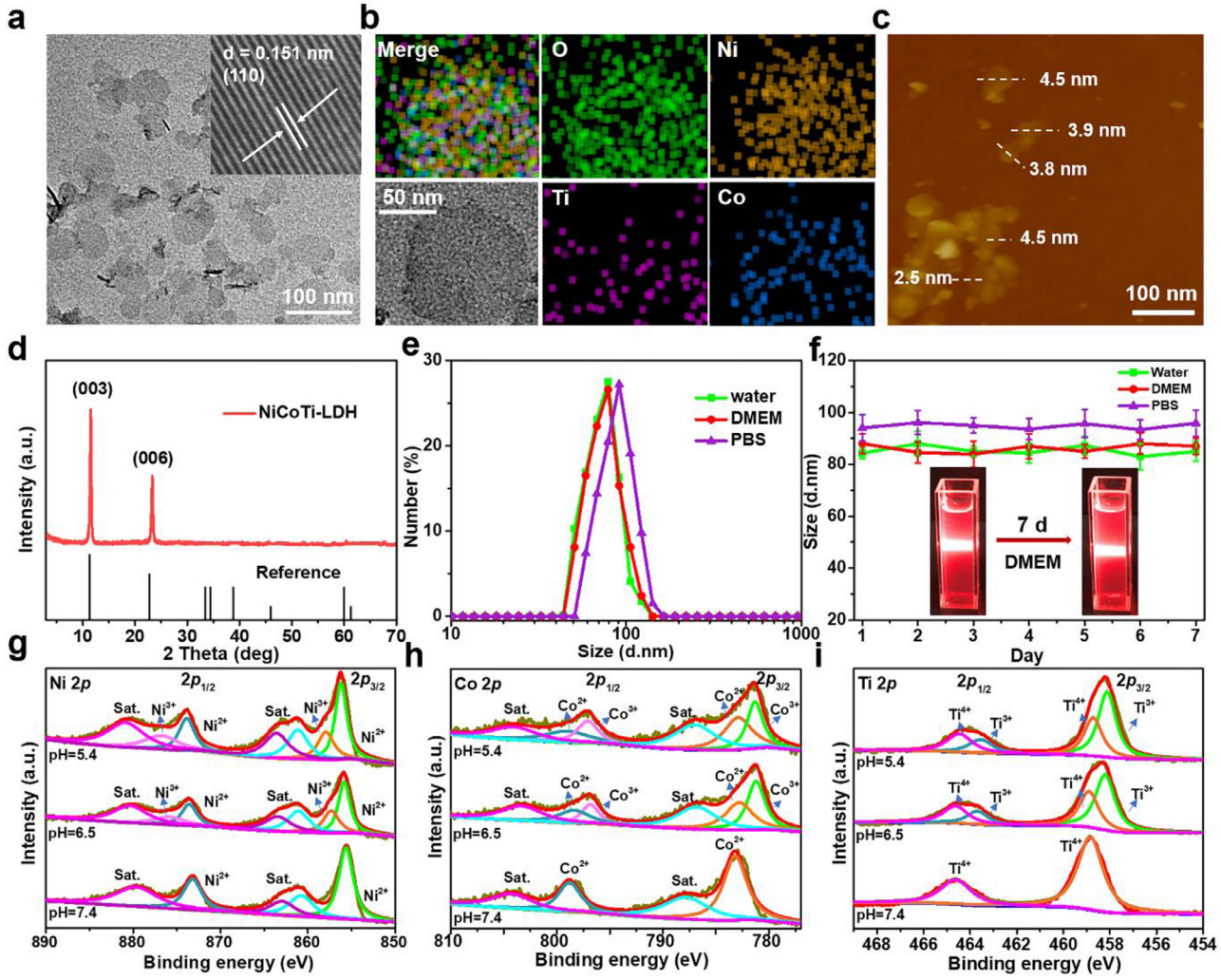

Fig. 1. Characterization of the NiCoTi-LDH nanosheets. (a) HRTEM image. (b) EDX mapping. (c) AFM image. (d) XRD patterns of NiCoTi-LDH nanosheets. (e) Size distribution of NiCoTi-LDH nanosheets in water, PBS and DMEM culture medium, respectively. (f) Stability tests in water, PBS and DMEM showing the particle sizes over 7 days. Data shown as mean ± s.d. (n = 3). (Insets show digital photographs of NiCoTi-LDH nanosheets dispersed in DMEM on day 1 and 7). (g) Ni 2p, (h) Co 2p and (i) Ti 2p XPS spectra of NiCoTi-LDH nanosheets at pH 7.4, 6.5, and 5.4.

photographs of NiCoTi-LDH nanosheets dispersed in high glucose Dulbecco's modified Eagles medium (DMEM), water and PBS are displayed in the inset in Fig. 1f and Fig. S1, respectively. X-ray photoelectron spectroscopy (XPS) was employed to confirm the valence state of Ni, Co and Ti in the nanosheets. The Ni 2p, Co 2p, O 1 s, and Ti 2p peaks are all found in the survey spectra (Fig. S2). Characteristic peaks with binding energies (BEs) at 855.65 eV and 873.21 eV in the high-resolution spectrum (Fig. 1g, pH 7.4) are assigned to Ni^{2+} $2p_{3/2}$ and $2p_{1/2}$ [29], and the peaks at 781.18 eV ($2p_{3/2}$), 785.84 eV ($2p_{3/2}$ satellite), 796.81 eV ($2p_{1/2}$) and 802.27 eV ($2p_{1/2}$ satellite) are attributed to Co^{2+} (Fig. 1h, pH 7.4) [30]. In the Ti 2p spectrum, two main peaks are observed at 458.10 eV ($2p_{3/2}$) and 463.60 eV ($2p_{1/2}$) (Fig. 1i, pH 7.4) [31], confirming the presence of Ti^{4+} in the NiCoTi-LDH nanosheets.

The absorption spectrum of the NiCoTi-LDH nanosheets was measured by an ultraviolet-visible-near-infrared (UV–vis-NIR) diffuse reflection spectrophotometer. The NiCoTi-LDH nanosheets show a broad and strong absorption in the range of 500 to 700 nm (Fig. S3a). Such result suggests that the NiCoTi-LDH nanosheets have the potential to be excited by visible light (650 nm). The photodynamic properties of NiCoTi-LDH nanosheets under 650 nm laser irradiation were studied by using 1,3-diphenylisobenzofuran (DPBF) as a detector (absorption band: 410 nm) and the traditional inorganic type I PS TiO_2 as a comparison [32]. As shown in Fig. S4, a gentle decline in the absorbance of the DPBF solution (6.3%) is observed upon 650 nm laser irradiation (100 mW cm^{-2}, 6 min) owing to its self-decomposition. The presence of NiCoTi-LDH nanosheets (pH 7.4) and TiO_2 accelerated this process with a decreased absorbance of 17.4% and 40.6%, respectively. In the case of NiCoTi-LDH nanosheets at pH 6.5, a decrease of 68.7% in absorbance is observed within 6 min. It is therefore concluded that the ROS generation ability of NiCoTi-LDH nanosheets under acidic conditions is stronger than that of TiO_2 and NiCoTi-LDH nanosheets in a neutral environment, indicating a strong pH-responsive PDT performance.

To further explore ROS generation by NiCoTi-LDH nanosheets, electron spin resonance (ESR) spectroscopy was applied using 5,5-dimethyl-1-pyrroline N-oxide (DMPO) as a spin probe for the detection of ·OH [33,34]. In Fig. 2a, obvious ·OH signals are observed when the NiCoTi-LDH suspension was in mildly acidic conditions (pH 6.5 and 5.4) under 650 nm laser irradiation (100 mW cm^{-2}, 10 min). Comparatively, almost no signal is found in identical measurement conditions at neutral pH (pH 7.4), confirming the pH-responsive PDT performance of NiCoTi-LDH nanosheets. As shown in Fig. 2b, with the introduction of H_2O_2, NiCoTi-LDH nanosheets at both pH 6.5 and 5.4 generated a considerable amount of ·OH while almost no ·OH signal was detected at pH 7.4, indicating the acid-enhanced CDT performance. Moreover,

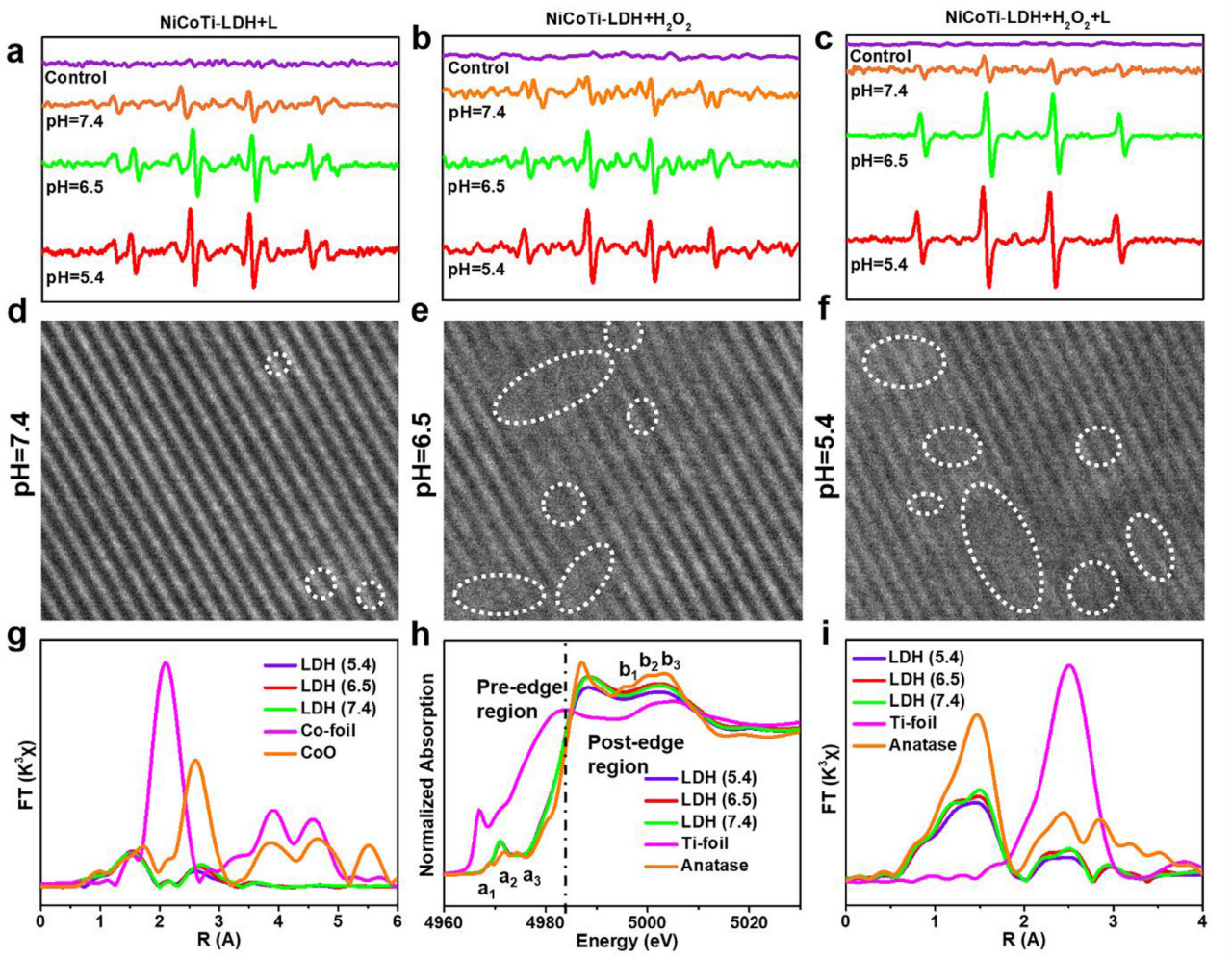

Fig. 2. ROS evaluation and fine-structure characterizations of the NiCoTi-LDH nanosheets. ESR spectra of DMPO/·OH for NiCoTi-LDH nanosheets (a) under 650 nm laser irradiation (100 mW cm^{-2}, 10 min) in buffers with various pH values, (b) with H_2O_2 in buffers with various pH values, (c) with H_2O_2 under laser irradiation. (d-f) Lattice fringes of NiCoTi-LDH nanosheets at pH 7.4, 6.5 and 5.4, respectively (the white dashed circles indicate lattice defects). (g) Fourier-transform Co *K*-edge EXAFS spectra of NiCoTi-LDH nanosheets (at pH 7.4, 6.5 and 5.4) and Co references. (h) Normalized Ti *K*-edge XANES spectra and (i) Fourier-transform Ti *K*-edge EXAFS spectra of NiCoTi-LDH nanosheets (at pH 7.4, 6.5 and 5.4) and Ti references.

the synergetic PDT/CDT performance of NiCoTi-LDH nanosheets was investigated. In mildly acidic conditions (pH 6.5 and 5.4), NiCoTi-LDH nanosheets co-existing with H_2O_2 displayed a significantly enhanced ·OH signal after laser irradiation compared with NiCoTi-LDH plus laser irradiation or H_2O_2 (Fig. 2c). All the above results illuminate the excellent ROS generation capability of NiCoTi-LDH nanosheets under acidic conditions and its potential in synergistic PDT/CDT. Considering that •OH can react with terephthalic acid (TA) to produce fluorescent 2-hydroxyterephthalic acid [35], we further utilized TA as a probe to detect •OH generated under the above conditions (Fig. S5), and the results are consistent with the ESR results.

To verify the reaction between NiCoTi-LDH and H_2O_2, XPS was applied to study the change in chemical state of Co after Fenton reaction. As shown in the Co 2*p* spectrum (Fig. S6a), four main peaks at 781.1 eV (Co^{3+} $2p_{3/2}$), 782.2 eV (Co^{2+} $2p_{3/2}$), 796.1 eV (Co^{3+} $2p_{1/2}$) and 797.5 eV (Co^{2+} $2p_{1/2}$) as well as two satellite peaks (787.5 eV and 803.0 eV) are observed, indicating that some Co^{2+} was oxidized to Co^{3+} in the presence of H_2O_2 with a Co^{2+}/Co^{3+} ratio ≈ 0.855 [36]. Subsequently, the reaction between NiCoTi-LDH and H_2O_2 under laser irradiation was also investigated and the molar ratio of Co^{2+}/Co^{3+} is found to be 1.261 (Fig. S6b). The above results reveal that the photoelectrons generated by NiCoTi-LDH nanosheets under photoexcitation accelerate the conversion of Co^{3+} to Co^{2+}. The consumption of H_2O_2 in the Fenton reaction without/with laser was evaluated through the formation of yellow titanium peroxide complex (TiO_2^{2+}) from titanic sulfate ($Ti(SO_4)_2$) (Fig. S7a and S7b) [37]. Compared with a control experiment without laser irradiation, NiCoTi-LDH consumed more H_2O_2 at pH 7.4, 6.5 and 5.4 when the laser was applied (Fig. S7c and S7d), implying a photoelectron-promoted Fenton reaction.

To explore the structure changes induced by different pH conditions, the NiCoTi-LDH nanosheets were characterized by HRTEM, ESR, XPS, Raman spectra, X-ray absorption near-edge structure (XANES) spectra and UV–vis-NIR spectroscopy. HRTEM images of the (110) lattice plane of NiCoTi-LDH were first characterized. After the nanosheets were treated with sodium acetate buffer for 0.5 h, few OVs are seen at pH 7.4 (Fig. 2d). In contrast, many OVs are found at pH 6.5 (Fig. 2e) and 5.4 (Fig. 2f), demonstrating that the weak acid environment etched the surface of NiCoTi-LDH nanosheets and caused abundant OVs. As shown in Fig. S8, the size of the NiCoTi-LDH nanosheets etched at pH 6.5 is slightly smaller than that at pH 6.5 (Fig. 1a), and the size becomes more smaller after the treatment of pH 5.4. Such results reveal that the NiCoTi-LDH nanosheets will be partially etched from the edges at the acidic conditions in addition to the generation of OVs. ESR spectra show a markedly stronger signal at $G = 2.002$ at pH 5.4 and 6.5 than at pH

7.4 (Fig. S9), indicating that defects are generated through acid etching [38,39]. The XPS analysis of NiCoTi-LDH nanosheets at pH 7.4, 6.5 and 5.4 is presented in Fig. 1g-i and S10. In Fig. 1g, the XPS Ni 2*p* spectra at pH 6.5 and 5.4 show four peaks at 855.86, 873.60, 857.34 and 875.82 eV, which can be attributed to Ni^{2+} $2p_{3/2}$, Ni^{2+} $2p_{1/2}$, Ni^{3+} $2p_{3/2}$, Ni^{3+} $2p_{1/2}$, respectively, proving the generation of Ni^{3+} at pH 6.5 and 5.4 compared to pH 7.4 [40]. Similarly, the Co 2*p* spectra at pH 6.5 and 5.4 show four peaks at 782.80 eV (Co^{2+} $2p_{3/2}$), 798.36 eV (Co^{2+} $2p_{1/2}$), 781.21 eV (Co^{3+} $2p_{3/2}$) and 796.85 eV (Co^{3+} $2p_{1/2}$), indicating the generation of Co^{3+} (Fig. 1h) [42]. In the Ti 2*p* spectra (Fig. 1i), at pH 6.5 and 5.4 characteristic peaks are located at 458.21 eV (Ti^{3+} $2p_{3/2}$), 463.69 eV (Ti^{3+} $2p_{1/2}$), 458.90 eV (Ti^{4+} $2p_{3/2}$) and 464.63 eV (Ti^{4+} $2p_{1/2}$), demonstrating the coexistence of Ti^{3+} and Ti^{4+} [40]. The O 1 *s* spectra indicate the existence of different oxygen species in NiCoTi-LDH nanosheets (Fig. S10). Compared with the binding energies located at 530.84 eV (O_L: lattice oxygen) and 532.35 eV (O_S: adsorbed oxygen) visible for the NiCoTi-LDH nanosheets at pH 7.4, a peak at 531.36 eV indicates the presence of extensive OVs at pH 6.5 and 5.4. Therefore, in an acid environment, OVs and changes in the valence states of Ni, Co, and Ti are induced. Raman spectra further confirmed the existence of OVs in NiCoTi-LDH nanosheets exposed to an acid environment (see Fig. S11). The spectra exhibit a non-symmetric peak at ~510 cm^{-1} (Ni-O stretching) and ~496 cm^{-1} (Ti-O torsional vibrations). These peak intensities are lower at pH 6.5 and 5.4 than at pH 7.4, suggesting the formation of OVs in the NiCoTi-LDH nanosheets.

XANES spectra (Figs. 2g-i and S12) were also carried out to reveal the structural information of NiCoTi-LDH nanosheets and the corresponding change of coordination environment under acidic conditions. As shown in Fig. 2g, the Fourier transformed (FT) $k^3\chi(k)$ Co *K*-edge EXAFS curves reveal a structural change in the coordination environment of Co atoms. Two main peaks at 1.6 and 2.8 Å are observed, corresponding to the nearest Co-OOH and next nearest Co···Co coordination, respectively. The peaks intensity of Co···Co coordination in NiCoTi-LDH at pH 6.5 and 5.4 is lower than that at pH 7.4, suggesting the formation of coordinatively unsaturated CoO_{6-x} octahedra with OVs under acidic conditions [41]. Fig. 2h illustrates the normalized Ti *K*-edge XANES spectra. The spectra are defined in two portions: the pre-edge region and post-edge region, with a white line peak at ~4987 eV [42,43]. Compared with anatase, the disappearance of three peaks (denoted as b_1, b_2, and b_3, within 4993–5006 eV) is attributed to the formation of distorted Ti-O octahedra related to OVs. Three pre-peaks (labeled as a_1, a_2, a_3) were also investigated. The a_2 pre-peak at pH 7.4, 6.5 and 5.4 strengthened and shifted to lower energy, demonstrating the presence of low-coordination number Ti species (from 6 to 5 coordination) [44]. The FT spectra presented in Fig. 2i indicates that the Ti-O coordination peak intensity at pH 6.5 and 5.4 is lower than that at pH 7.4, proving the pH-responsive generation of OVs.

The band structure of the NiCoTi-LDH nanosheets was determined by UV–vis-NIR diffuse reflectance spectra (see Fig. S3). The bandgaps (E_g) at pH 7.4, 6.5 and 5.4 are calculated to be 2.38 eV, 1.88 eV, and 1.62 eV, respectively, which means that the generation of OVs decreases the E_g. This explains why the NiCoTi-LDH nanosheets at pH 6.5 and 5.4 can be effectively excited by visible light (650 nm) to exert a PDT performance. The photoluminescence properties were recorded (Fig. S13) to elucidate the recombination of photogenerated charges, which indirectly reveals the transfer and separation efficiency of electron-hole pairs [45]. The peak intensity of NiCoTi-LDH nanosheets at pH 6.5 and 5.4 is obviously weaker than that at pH 7.4, indicating inhibited recombination efficiency of photogenerated charges after the generation of OVs under acidic conditions.

Inspired by the results discussed above, we explored the anticancer effect of NiCoTi-LDH nanosheets *in vitro*. Prior to this, HeLa cells (human cervical cancer cells) incubated with NiCoTi-LDH nanosheets labeled with Cy5.5 dye were imaged using a fluorescence microscope (Fig. 3a). Obvious fluorescence intensity inside the HeLa cells was observed after incubation for 12 h, demonstrating the cellular uptake of the LDH nanosheets. The mechanism of LDH uptake could be explained as that LDH nanosheets were internalized by HeLa cells *via* clathrin-mediated endocytosis, and then delivered into cytoplasm *via* endosomal escape [46]. The *in vitro* biocompatibility of NiCoTi-LDH nanosheets was then tested on two kinds of cancerous cells (HeLa and HepG2: human hepatoma carcinoma cell) and two kinds of normal healthy cells (Cos-7: African green monkey kidney fibroblasts and MREpiC: mouse renal epithelial cells) *via* the standard methyl thiazolyl tetrazolium (MTT) assay as well as by calcein acetoxymethyl ester and propidium iodide (Calcein-AM/PI) staining [47]. The results indicate that the NiCoTi-LDH nanosheets exhibit nontoxic behavior to these cells even at a high concentration of 100 $\mu g\ mL^{-1}$ (Fig. S14).

In vitro cytotoxicity induced by NiCoTi-LDH nanosheets was investigated in normoxia (21% O_2) and hypoxia (1% O_2). The viability of HeLa cells after different treatments under hypoxia (Fig. 3b and 3c) is similar to that under normoxia (Fig. S15). However, in hypoxia conditions with the addition of H_2O_2 (100 μM), HeLa cells incubated with NiCoTi-LDH nanosheets (30 $\mu g\ mL^{-1}$) exhibit much lower viability at pH 6.5 (69.0 ± 3.7%) than at pH 7.4 (92.1 ± 2.6%), demonstrating the pH-responsive CDT performance. The viability of HeLa cells treated with NiCoTi-LDH nanosheets and exposed to laser irradiation (100 mW cm^{-2}, 10 min) is found to be 43.1 ± 4.1% (pH 6.5) *vs* 84.8 ± 3.6% (pH 7.4), suggesting the LDH to provide pH-responsive PDT performance. Subsequently, the synergetic PDT/CDT efficiency of NiCoTi-LDH nanosheets was investigated. HeLa cells treated with NiCoTi-LDH nanosheets are very efficiently killed under irradiation in the presence of H_2O_2. The viabilities are found to be 72.4 ± 2.1% and 8.1 ± 1.7% at pH 7.4 and pH 6.5, respectively, demonstrating a synergistic PDT/CDT performance of NiCoTi-LDH under hypoxic acid conditions with irradiation. Calcein-AM/PI staining was applied to visualize the distribution of living and dead cells under hypoxia. As shown in Fig. 3d, at pH 6.5 in the presence of H_2O_2 the LDH nanosheets cause the maximum cell death, consistent with the MTT assay results.

In vitro ROS generation under hypoxia was further evaluated by introducing 2′, 7′-dichlorodihydrofluorescein diacetate (DCFH-DA) as a ROS fluorescent probe [48]. As illustrated in Fig. 3e, almost no fluorescence is observed in confocal laser scanning microscopy (CLSM) images of NiCoTi-LDH-treated HeLa cells at pH 7.4 and pH 6.5. The fluorescence signal with H_2O_2 at pH 6.5 is stronger than that at pH 7.4. Under irradiation (100 mW cm^{-2}, 10 min), stronger green fluorescence is observable at pH 6.5 than at pH 7.4. For H_2O_2 and NiCoTi-LDH nanosheets co-treated HeLa also exposed to laser irradiation, the green fluorescence is the strongest at pH 6.5, confirming of pH-responsive PDT/CDT. Corresponding intracellular fluorescence-intensity profiles were collected and quantified in Fig. S16a, b.

As cell death is often accompanied by intracellular organelle disruption, the damage caused by PDT, CDT and PDT/CDT on lysosomes and mitochondria was investigated under hypoxia. Acridine orange (AO) was adopted as a lysosomal integrity indicator to monitor the lysosomal membrane permeabilization (LMP) of HeLa cells [26] (Fig. 3f). The orange fluorescence signal in the cytoplasm increases gradually after the treatment with CDT (NiCoTi-LDH plus H_2O_2), PDT (NiCoTi-LDH plus laser), and synergistic PDT/CDT (NiCoTi-LDH plus H_2O_2 and laser) respectively, indicating LMP-triggered release of lysosomal content into the cytoplasm. In the PDT/CDT group, the fluorescence signal is the strongest and the nuclear morphology is significantly diminished and atrophied, indicating ROS-mediated lysosome destruction. Subsequently, we assessed the mitochondrial dysfunction by using the 5,5′,6,6′-tetrachloro-1,1′−3,3′-tetraethyl-benzimidazolylcarbocyanine iodide (JC-1) probe to reflect the changes of mitochondrial membrane potential (MMP) [49] (Fig. 3g). A gradual decrease in MMP is observed in CDT-, PDT-, and PDT/CDT-treated cells, as indicated by the decreased red/green fluorescence ratio of JC-1. The collapse of MMP is most pronounced in PDT/CDT group, demonstrating ROS-mediated mitochondrial membrane depolarization. The synergistic PDT/CDT anticancer efficacy of the NiCoTi-LDH

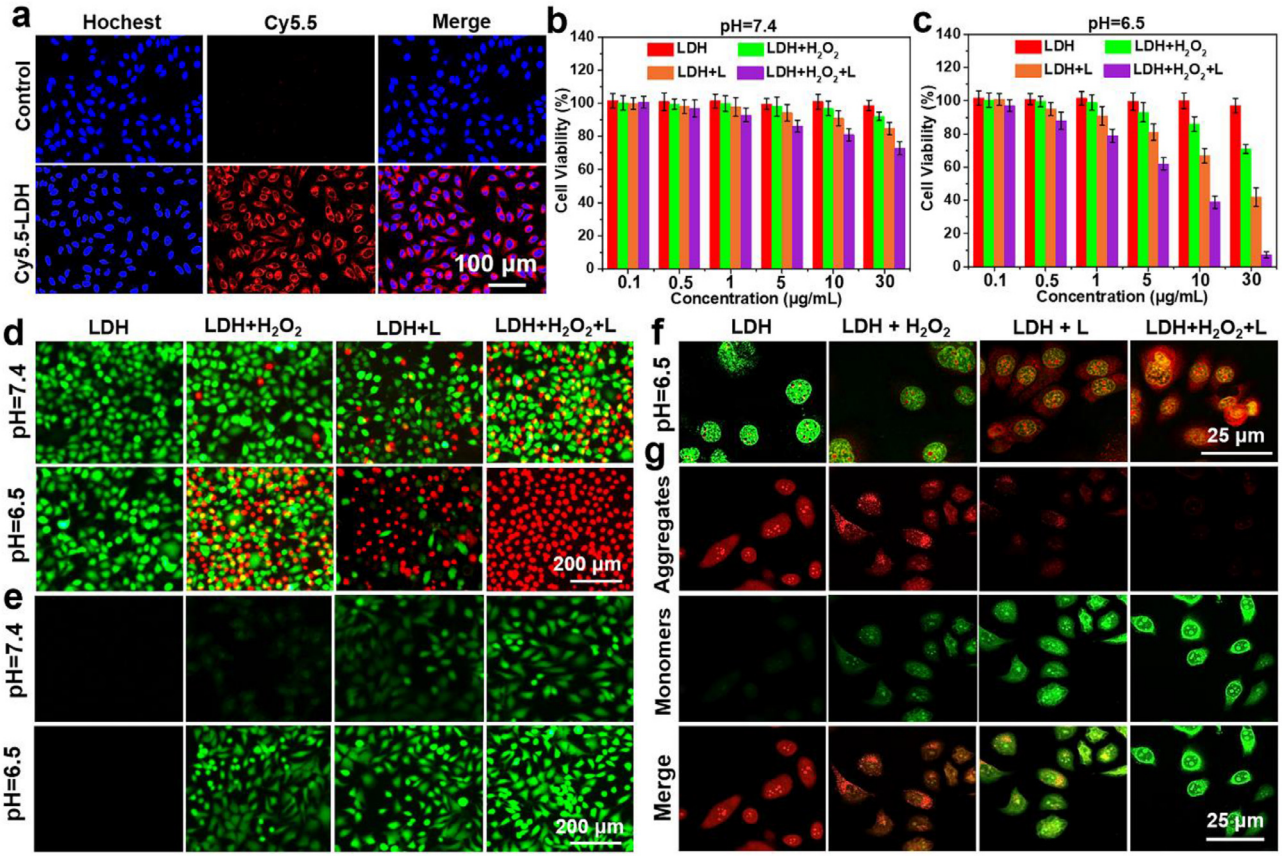

Fig. 3. ***In vitro*** **therapeutic effect of the NiCoTi-LDH nanosheets with Hela cells.** (a) Fluorescence images of HeLa cells treated by NiCoTi-LDH nanosheets (30 μg mL^{-1}). *In vitro* cytotoxicity profiles of cells incubated with NiCoTi-LDH nanosheets under hypoxic (b) neutral (pH 7.4) and (c) acidic (pH 6.5) conditions: (1) LDH, (2) LDH + H_2O_2 (100 μM), (3) LDH + 650 nm laser (100 mW cm^{-2} for 10 min), (4) LDH + H_2O_2 (100 μM) + 650 nm laser, and (d) corresponding Calcein-AM/PI staining images. (e) ROS fluorescence probe DCFH-DA staining images of cells after incubation with NiCoTi-LDH nanosheets (30 μg mL^{-1}) in the same conditions as MTT assays. (f) CLSM images of AO staining for lysosomal integrity after different treatments. (g) Mitochondrial membrane depolarization of cells incubated with NiCoTi-LDH nanosheets under hypoxic acid (pH 6.5) conditions. Quantitative data shown as mean ± s.d. (n = 3).

nanosheets was analyzed using a quantitative cell apoptosis assay (Fig. S17). Cells were stained by Annexin V-FITC/PI, revealing that both PDT and CDT led to early-stage apoptosis of HeLa cells. In the presence of H_2O_2, cells incubated with NiCoTi-LDH nanosheets at pH 6.5 under irradiation show almost complete apoptosis.

Encouraged by the promising *in vitro* results, *in vivo* experiments were performed on female BALB/c nude mice. Firstly, the pharmacokinetics of NiCoTi-LDH nanosheets was examined by measuring the Ni concentration in the blood at different time points post-injection (5 mg kg^{-1}, 200 μL). As illustrated in Fig. 4a, the blood circulation of NiCoTi-LDH follows a two-compartment model, with a half-life time of 1.16 ± 0.16 h in the distribution phase and 15.79 ± 1.02 h in the elimination phase, indicating an extended blood circulation time. To quantitatively measure the biodistribution, HeLa tumor-bearing mice injected with NiCoTi-LDH nanosheets were sacrificed at different time points, and their major organs (heart, liver, spleen, lung, and kidney) and tumors were harvested. After weighing and digestion, the content of Ni in the major organs and tumors was determined by inductively coupled plasma-mass spectrometry (ICP-AES). The results show that NiCoTi-LDH nanosheets could accumulate in the tumor. The maximum accumulation appeared at 12 h post-injection, which is due to the enhanced permeability and retention (EPR) effect (Fig. 4b).

PDT/CDT therapy based on NiCoTi-LDH nanosheets was investigated through an *in vivo* tumoricidal experiment. 18 HeLa tumor-bearing mice were randomly separated into 3 groups: (1) control group (PBS + 650 nm laser), (2) CDT group (NiCoTi-LDH), and (3) PDT/CDT group (NiCoTi-LDH + 650 nm laser). The mice in groups 1 and 3 were exposed to a 650 nm laser (100 mW cm^{-2}, 10 min) at 12 h after intravenous administration of PBS or NiCoTi-LDH nanosheets (5 mg kg^{-1}, 200 μL). The tumor volume was monitored continuously over the following 16 days, and the corresponding tumor growth curves are shown in Fig. 4c. The tumor volume of the mice in the PBS + laser group increases rapidly, while in the NiCoTi-LDH group growth is somewhat suppressed, indicating the anti-tumor effect of CDT treatment. However, the tumor growth in the NiCoTi-LDH + laser group is inhibited much more completely, indicating a very strong PDT/CDT synergistic effect from the NiCoTi-LDH nanosheets. These results were validated by digital photos of the mice (Fig. 4d) and the excised tumors (Fig. 4e).

We utilized the standard droethidium (DHE) staining assay to determine the ROS production efficacy of PDT/CDT *ex vivo* [50] (see Fig. 4f). No obvious red fluorescence is observed in the PBS + laser group, but some is visible in the NiCoTi-LDH group, confirming the LDH has notable CDT properties. The fluorescence intensity in the tumor slices of NiCoTi-LDH + laser group is the strongest, implying that NiCoTi-LDH nanosheets could generate significant amounts of ROS under laser irradiation. Hematoxylin and eosin (H&E) and terminal deoxynucleotidyl transferase (TdT)-mediated deoxyuridine triphosphate (dUTP) nick end labeling (TUNEL) staining were carried out to study the morphology of the tumor tissues (Fig. 4g). Tumor tissues from mice treated with NiCoTi-LDH + laser exhibit the most obvious necrosis compared with the other two groups, consistent with Fig. 4d and 4e.

Finally, to aid the translation from laboratory bench to clinical applications, the toxicity of the NiCoTi-LDH nanosheets *in vivo* was evaluated. Bodyweight changes in all mice were negligible during the 16-day exper-

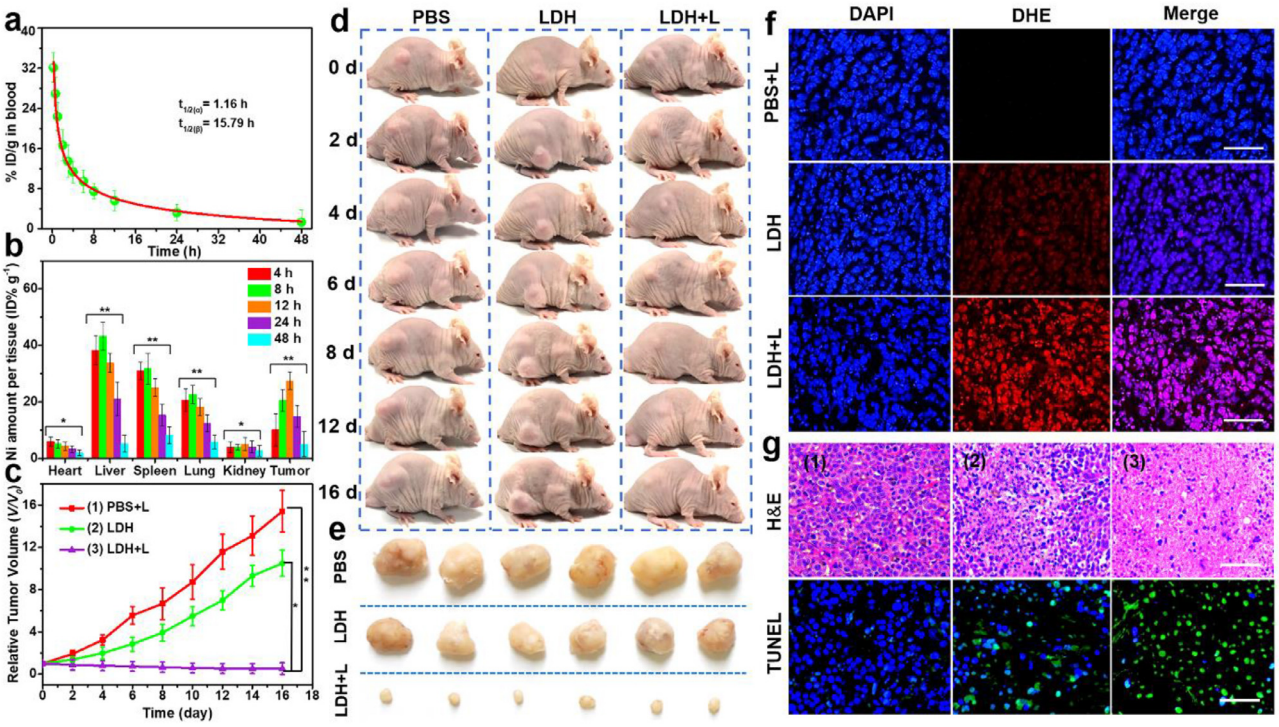

Fig. 4. *In vivo* therapeutic effect of the NiCoTi-LDH nanosheets conducted on Hela tumor bearing mice. (a) Blood circulation time of the NiCoTi-LDH nanosheets. (b) Quantitative biodistribution analysis of NiCoTi-LDH nanosheets in mice by measuring the Ni concentration at various time points post-injection. Data shown as mean ± s.d. (n = 3). (c) Tumor growth curves of mice given various treatments ($^{*}p < 0.05$, $^{**}p < 0.01$). Tumor sizes were normalized to their initial sizes (n = 6 per group). Data shown as mean ± s.d. (n = 6). (d) Representative photographs of mice at different time points and (e) corresponding images of tumors taken on day 16. (f) DHE staining and (g) H&E and TUNEL staining assay of tumor tissue slices from different groups of mice after 16-d treatment: (1) PBS + 650 nm laser, (2) NiCoTi-LDH, (3) NiCoTi-LDH + 650 nm laser. Scale bars are 100 μm.

iment (Fig. S18). After 1 and 16 d post-injection, routine blood examinations were performed to measure the levels of key biomarkers and further evaluate the *in vivo* biocompatibility of NiCoTi-LDH nanosheets. As presented in Fig. S19, the blood biochemistry, liver and kidney function markers in mice treated with NiCoTi-LDH nanosheets are all within the normal range and similar to those in the control group, demonstrating no evident toxicity of inflammation caused by the NiCoTi-LDH nanosheets. The biocompatibility of the nanosheets was verified by H&E staining of the major organs (Fig. S20); these show no changes after LDH treatment compared to the control, confirming there to be no significant off-target adverse effects of NiCoTi-LDH *in vivo*.

3. Conclusion

A novel inorganic nanoagent based on ternary NiCoTi-LDH nanosheets has been prepared for the first time to realize pH-responsive and highly efficient PDT/CDT synergistic therapy. The NiCoTi-LDH nanosheets could generate electron-hole pairs under laser irradiation to produce ·OH, and their efficacy as PDT agents could be markedly increased in an acid environment owing to OV-facilitated photoelectron-hole pair separation. The separated photogenerated electrons could accelerate the conversion between Co^{3+} and Co^{2+}, enabling the NiCoTi-LDH nanosheets to catalyze the disproportionation of H_2O_2 into ·OH at the tumor site. The NiCoTi-LDH nanosheets can thus further act as a CDT agent. The combination of OV-facilitated PDT and photoelectron-promoted CDT led to a considerable amount of ROS generation and consequently tumor-cell apoptosis and death. The *in vivo* therapeutic results revealed that under laser irradiation, they led to a highly potent tumor-suppression effect towards a HeLa tumor xenograft. This study has proven that the NiCoTi-LDH nanosheets could trigger the production of electron-hole pairs and accelerate the Fenton reaction in response to the conditions in the tumor microenvironment, with exogenous laser irradiation further inhibiting tumor growth. This study on pH-responsive ternary NiCoTi-LDH nanosheets provides a promising example for tumor treatment with enhanced effectiveness and specificity.

Declaration of Interest Statement

The authors declare that they have no conflicts of interest in this work.

Acknowledgments

R.L. thanks the funding support from National Natural Science Foundation of China (Grant No: 21971007) and the Beijing Natural Science Foundation (Grant No. 2212044). C.T. thanks the funding support from the National Natural Science Foundation of China (Grants No. 52122002 and 22005259) and the Start-Up Grant (Grant No. 9610495) from City University of Hong Kong.

Supplementary materials

Supplementary material associated with this article can be found, in the online version, at doi:10.1016/j.fmre.2022.06.001.

References

[1] Q. Tian, F. Xue, Y. Wang, et al., Recent advances in enhanced chemodynamic therapy strategies, Nano Today 39 (2021) 101162.
[2] Z. Tang, Y. Liu, M. He, et al., Chemodynamic therapy: tumour microenvironment-mediated Fenton and Fenton-like reactions, Angew. Chem. Int. Ed. 58 (4) (2019) 946–956.
[3] Y. Yang, Z. Liu, Chemiluminescent nanosystems for imaging cancer chemodynamic therapy, Chem 6 (9) (2020) 2127–2129.
[4] T.J. Zhou, Y. Xu, L. Xing, et al., A harmless-harmful switchable and uninterrupted laccase-instructed killer for activatable chemodynamic therapy, Adv. Mater. 33 (27) (2021) 2100114.

[5] K. Yang, G. Yu, Z. Yang, et al., Supramolecular polymerization-induced nanoassemblies for self-augmented cascade chemotherapy and chemodynamic therapy of tumor, Angew. Chem. Int. Ed. 60 (32) (2021) 17570–17578.
[6] H. Deng, Z. Yang, X. Pang, et al., Self-sufficient copper peroxide loaded pKa-tunable nanoparticles for lysosome-mediated chemodynamic therapy, Nano Today 42 (2022) 101337.
[7] L. Zhang, S.S. Wan, C.X. Li, et al., An adenosine triphosphate-responsive autocatalytic Fenton nanoparticle for tumor ablation with self-supplied H_2O_2 and acceleration of Fe(III)/Fe(II) conversion, Nano Lett 18 (12) (2018) 7609–7618.
[8] X. Nie, L. Xia, H.L. Wang, et al., Photothermal therapy nanomaterials boosting transformation of Fe(III) into Fe(II) in tumor cells for highly improving chemodynamic therapy, ACS Appl. Mater. Interfaces 11 (35) (2019) 31735–31742.
[9] X. Li, B.D. Zheng, X.H. Peng, et al., Phthalocyanines as medicinal photosensitizers: developments in the last five years, Coord. Chem. Rev. 379 (2019) 147–160.
[10] M. Yang, T. Yang, C. Mao, Enhancement of photodynamic cancer therapy by physical and chemical factors, Angew. Chem. Int. Ed. 58 (40) (2019) 14066–14080.
[11] L. Huang, S. Zhao, J. Wu, et al., Photodynamic therapy for hypoxic tumors: advances and perspectives, Coord. Chem. Rev. 438 (2021) 213888.
[12] T.C. Pham, V.N. Nguyen, Y. Choi, et al., Recent strategies to develop innovative photosensitizers for enhanced photodynamic therapy, Chem. Rev. 121 (21) (2021) 13454–13619.
[13] H. Ranji-Burachaloo, P.A. Gurr, D.E. Dunstan, et al., Cancer treatment through nanoparticle-facilitated Fenton reaction, ACS Nano 12 (12) (2018) 11819–11837.
[14] G. Ruppert, R. Bauer, G. Heisler, The photo-Fenton reaction-an effective photochemical wastewater treatment process, J. Photochem. Photobiol. A: Chem. 73 (1) (1993) 75–78.
[15] B.C. Faust, J. Hoigné, Photolysis of Fe (III)-hydroxy complexes as sources of OH radicals in clouds, fog and rain, Atmospheric Environment. Part A. General Topics 24 (1) (1990) 79–89.
[16] X. Ji, Y. Kang, J. Ouyang, et al., Synthesis of ultrathin biotite nanosheets as an intelligent theranostic platform for combination cancer therapy, Adv. Sci. 6 (19) (2019) 1901211.
[17] J. Kim, H.R. Cho, H. Jeon, et al., Continuous O_2-evolving $MnFe_2O_4$ nanoparticle-anchored mesoporous silica nanoparticles for efficient photodynamic therapy in hypoxic cancer, J. Am. Chem. Soc. 139 (32) (2017) 10992–10995.
[18] E. Ju, K. Dong, Z. Chen, et al., Copper(II)-graphitic carbon nitride triggered synergy: improved ROS generation and reduced glutathione levels for enhanced photodynamic therapy, Angew. Chem. Int. Ed. 55 (38) (2016) 11467–11471.
[19] P. Hu, T. Wu, W. Fan, et al., Near infrared-assisted Fenton reaction for tumor-specific and mitochondrial DNA-targeted photochemotherapy, Biomaterials 141 (2017) 86–95.
[20] Z. Cao, B. Li, L. Sun, et al., 2D layered double hydroxide nanoparticles: recent progress toward preclinical/clinical nanomedicine, Small Methods 4 (2) (2020) 1900343.
[21] V.K. Shirin, R. Sankar, A.P. Johnson, et al., Advanced drug delivery applications of layered double hydroxide, J. Control. Release 330 (2021) 398–426.
[22] B. Li, Z. Gu, N. Kurniawan, et al., Manganese-based layered double hydroxide nanoparticles as a T_1-MRI contrast agent with ultrasensitive pH response and high relaxivity, Adv. Mater. 29 (29) (2017) 1700373.
[23] J. Liu, Y. Wu, C. Fu, et al., Charge reversion simultaneously enhances tumor accumulation and cell uptake of layered double hydroxide nanohybrids for effective imaging and therapy, Small 16 (31) (2020) 2002115.
[24] L. Peng, X. Mei, J. He, et al., Monolayer nanosheets with an extremely high drug loading toward controlled delivery and cancer theranostics, Adv. Mater. 30 (16) (2018) 1707389.
[25] X. Mei, T. Hu, H. Wang, et al., Highly dispersed nano-enzyme triggered intracellular catalytic reaction toward cancer specific therapy, Biomaterials 258 (2020) 120257.
[26] T. Hu, L. Yan, Z. Wang, et al., A pH-responsive ultrathin Cu-based nanoplatform for specific photothermal and chemodynamic synergistic therapy, Chem. Sci. 12 (7) (2021) 2594–2603.
[27] R. Gao, X. Mei, D. Yan, et al., Nano-photosensitizer based on layered double hydroxide and isophthalic acid for singlet oxygenation and photodynamic therapy, Nat. Commun. 9 (2018) 2798.
[28] J. Wu, S. Zhang, X. Mei, et al., Ultrathin transition metal chalcogenide nanosheets synthesized via topotactic transformation for effective cancer theranostics, ACS Appl. Mater. Inter. 12 (43) (2020) 48310–48320.
[29] H. Li, L. Zhang, Y. Mao, et al., A simple electrochemical route to access amorphous Co-Ni hydroxide for non-enzymatic glucose sensing, Nanoscale Res. Lett. 14 (2019) 135.
[30] Q. Yin, D. Rao, G. Zhang, et al., CoFe-Cl layered double hydroxide: a new cathode material for high-performance chloride ion batteries, Adv. Funct. Mater. 29 (36) (2019) 1900983.
[31] D. Wang, N. Ge, T. Yang, et al., NIR-triggered crystal phase transformation of Ni-Ti-layered double hydroxides films for localized chemothermal tumor therapy, Adv. Sci. 5 (4) (2018) 1700782.
[32] R. Liang, R. Tian, L. Ma, et al., A supermolecular photosensitizer with excellent anticancer performance in photodynamic therapy, Adv. Funct. Mater. 24 (21) (2014) 3144–3151.
[33] S. Wang, Z. Wang, G. Yu, et al., Tumor-specific drug release and reactive oxygen species generation for cancer chemo/chemodynamic combination therapy, Adv. Sci. 6 (5) (2019) 1801986.
[34] Y. Chong, C. Ge, G. Fang, et al., Crossover between anti- and pro-oxidant activities of graphene quantum dots in the absence or presence of light, ACS Nano 10 (9) (2016) 8690–8699.
[35] Y. Liu, Q. Jia, Q. Guo, et al., Simultaneously activating highly selective ratiometric MRI and synergistic therapy in response to intratumoral oxidability and acidity, Biomaterials 180 (2018) 104–116.
[36] H. Liu, S. Cao, J. Zhang, et al., Facile control of surface reconstruction with Co^{2+} or Co^{3+}-rich (oxy)hydroxide surface on ZnCo phosphate for large-current-density hydrogen evolution in alkali, Mater. Today Phys. 20 (2021) 100448.
[37] S. Gao, Y. Jin, K. Ge, et al., Self-supply of O_2 and H_2O_2 by a nanocatalytic medicine to enhance combined chemo/chemodynamic therapy, Adv. Sci. 6 (24) (2019) 1902137.
[38] Z. Zhou, X. Wang, H. Zhang, et al., Activating layered metal oxide nanomaterials via structural engineering as biodegradable nanoagents for photothermal cancer therapy, Small 17 (12) (2021) 2007486.
[39] Z. Zhou, Y. Wang, F. Peng, et al., Intercalation-activated layered MoO_3 nanobelts as biodegradable nanozymes for tumor-specific photo-enhanced catalytic therapy, Angew. Chem. Int. Ed. 61 (16) (2022) e202115939.
[40] Y. Zhao, X. Jia, G. Chen, et al., Ultrafine NiO nanosheets stabilized by TiO_2 from monolayer NiTi-LDH precursors: an active water oxidation electrocatalyst, J. Am. Chem. Soc. 138 (20) (2016) 6517–6524.
[41] Q. Wang, L. Chen, S. Guan, et al., Ultrathin and vacancy-rich CoAl-layered double hydroxide/graphite oxide catalysts: promotional effect of cobalt vacancies and oxygen vacancies in alcohol oxidation, ACS Catal 8 (4) (2018) 3104–3115.
[42] M. Xu, S. He, H. Chen, et al., TiO_{2-x}-modified Ni nanocatalyst with tunable metal–support interaction for water-gas shift reaction, ACS Catal 7 (11) (2017) 7600–7609.
[43] C. Belver, R. Bellod, S.J. Stewart, et al., Nitrogen-containing TiO_2 photocatalysts: part 2. Photocatalytic behavior under sunlight excitation, Appl. Catal. B 65 (3–4) (2006) 309–314.
[44] N. Liu, M. Xu, Y. Yang, et al., $Au^{\delta-}$-Ov-Ti^{3+} interfacial site: catalytic active center toward low-temperature water gas shift reaction, ACS Catal 9 (4) (2019) 2707–2717.
[45] K. Zhao, Z. Zhang, Y. Feng, et al., Surface oxygen vacancy modified Bi_2MoO_6/MIL-88B (Fe) heterostructure with enhanced spatial charge separation at the bulk & interface, Appl. Catal. B 268 (2020) 118740.
[46] J. Liu, L. Sun, L. Li, et al., Synergistic cancer photochemotherapy via layered double hydroxide-based trimodal nanomedicine at very low therapeutic doses, ACS Appl. Mater. Interfaces 13 (6) (2021) 7115–7126.
[47] Z. Zhou, B. Li, C. Shen, et al., Metallic 1T phase enabling MoS_2 nanodots as an efficient agent for photoacoustic imaging guided photothermal therapy in the near-infrared-II window, Small 16 (43) (2020) 2004173.
[48] X. Wan, H. Zhong, W. Pan, et al., Programmed release of dihydroartemisinin for synergistic cancer therapy using a $CaCO_3$ mineralized metal-organic framework, Angew. Chem. Int. Ed. 58 (40) (2019) 14134–14139.
[49] J.H. Liang, Y. Zheng, X.W. Wu, et al., A tailored multifunctional anticancer nanodelivery system for ruthenium-based photosensitizers: tumor microenvironment adaption and remodeling, Adv. Sci. 7 (1) (2020) 1901992.
[50] W. Park, B.C. Bae, K. Na, A highly tumor-specific light triggerable drug carrier responds to hypoxic tumor conditions for effective tumor treatment, Biomaterials 77 (2016) 227–234.

Tingting Hu graduated from Beijing University of Chemical Technology (BUCT) with bachelor degree in 2018. She is now pursuing her PhD degree under the supervision of Prof. Ruizheng Liang at BUCT. Her current interests is on layered double hydroxide (LDH)-based biomaterials for cancer diagnosis and treatment.

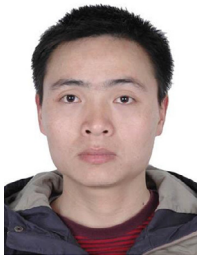

Chaoliang Tan is currently an Assistant Professor in the Department of Electrical Engineering at the City University of Hong Kong. He received his PhD from Nanyang Technological University in 2016. After working as a Research Fellow in the same group for about one year, he then worked as a Postdoctoral Researcher at the University of California, Berkeley, for two years. His-research focuses on 2D materials for electroncis and optoelectroncis as well as engineering of layered materials for biomedicine, energy storage, etc. He received the NSFC Excellent Young Scientist Fund (HK & Macau) in 2021.